INSTITUTE OF PHYSICS PUBLISHING MEASUREMENT SCIENCE AND TECHNOLOGY
Meas. Sci. Technol. **14** (2003) 1839–1844 PII: S0957-0233(03)59309-2

An analysis of complex electromagnetic radiation signals induced by fracture

J Goldbaum[1], V Frid[2], D Bahat[2] and A Rabinovitch[1]

[1] Department of Physics, The Deichmann Rock Mechanics Laboratory of the Negev, Ben Gurion University of the Negev, Beer Sheva, Israel
[2] Department of Geological and Environmental Sciences, The Deichmann Rock Mechanics Laboratory of the Negev, Ben Gurion University of the Negev, Beer Sheva, Israel

E-mail: julia@bgumail.bgu.ac.il

Received 6 February 2003, in final form and accepted for publication 30 July 2003
Published 2 September 2003
Online at stacks.iop.org/MST/14/1839

Abstract
As shown at the Laboratory of Rock Mechanics, electromagnetic radiation (EMR) emitted by propagating fractures provides relatively accurate information on the dimensions of the cracks emitting it. In this paper we demonstrate that this method (i.e. EMR analysis) can also be advantageously used for obtaining the exact time sequence of double or triple pulses when they appear simultaneously and, hence, the sequence of the relevant cracks. The method is first used to analyse the time sequence of a triple fracture during failure and for a double fracture in relaxation of a glass ceramic sample. The analysis is in good agreement with the actual fractography of the sample. A similar procedure applied to fracture of chalk enabled us to show that most large fractures are, in fact, double, and to find the specific time sequences involved.

Keywords: electromagnetic radiation, multiple cracks, multiple pulses, fractography

1. Introduction

It is established that fracturing excites electromagnetic radiation (EMR) [1–7]. In recent years, EMR emanating in uniaxial and triaxial compression of granite, rhyolite, chalk and glass ceramics [8–13], and also during percussion drilling of glass, PMMA, granite, Solenhofen and chalk [14], have been investigated. Some progress has been made in building a reliable model of EMR [11, 15]. The model is based on the analysis of single pulses, each of them having the form [10] given by the following equations (see figure 1)

$$A(t) = \begin{cases} A_0 \sin\omega(t-t_0) \\ \quad \times \left[1 - \exp\left(-\dfrac{t-t_0}{\tau_1}\right)\right], & t_0 < t < T \\ A_0 \sin\omega(t-t_0) \\ \quad \times \left[1 - \exp\left(-\dfrac{T-t_0}{\tau_1}\right)\right] \\ \quad \times \exp\left(-\dfrac{t-T}{\tau_2}\right), & t > T. \end{cases} \tag{1}$$

Here A_0 is the maximum amplitude of the pulse, t_0 is its onset time and T is the time to reach the maximum value of the amplitude; ω is the pulse frequency, τ_1 and τ_2 are the rise and the fall times respectively. It has been shown [16] that the rise and fall times of the same pulse are equal, $\tau_1 = \tau_2 = \tau$. The model implies that the time elapsed from the pulse onset to its maximum, which is denoted by $T' = T - t_0$, is proportional to the crack length L [10],

$$L = T' v_{\mathrm{cr}} \tag{2}$$

(v_{cr} is the crack propagation velocity), while the pulse frequency ω is inversely proportional to the crack width b,

$$\omega_{\mathrm{c}} = \frac{\pi v_{\mathrm{R}}}{b} \tag{3}$$

(v_{R} is Rayleigh velocity) [10].

The latter formula is valid for a crack closed on both sides; then its width equals half of a wavelength [10]. However, if the crack is open on one side, the crack width is a quarter rather than a half of a wavelength, namely

$$\omega_{\mathrm{o}} = \frac{\pi v_{\mathrm{R}}}{2b}. \tag{4}$$

It has been proven that the analysis of single EMR pulses presents information about the cracks they were emitted by. In some cases, however, more complicated pulses, e.g. double pulses or even triple pulses, are observed [17]. The objective of this paper is to examine these complicated pulses in order to understand their origin and to extract additional information about cracks that they can provide.

2. Equipment and method

The experimental compression system (see figure 2) consists of the following:

(a) A triaxial load frame (TerraTek stiff press model, axial load up to 450 MPa). Its stiffness is 5×10^9 N m^{-1}. It is combined with a closed-loop servocontrol with a linearity of 0.05%, which is used for axial piston displacement monitoring. The load is measured by a sensitive load cell (LC-222M, maximum capacity 220 kN, linearity 0.5% full scale). An axial cantilever (strain range about 10%; linearity 1% full scale) is used to measure sample strain parallel to uniaxial stress.
(b) A magnetic one-loop antenna 3 cm in diameter (EHFP-30 near field probe set, Electro-Metrics Penril Corporation). It is electrically small and wound within a balanced Faraday shield which makes its response to external electric fields vanishingly small.
(c) Low-noise micro-signal amplifier (Mitek Corporation Ltd, frequency range 10 kHz–500 MHz, gain 60 ± 0.5 dB, noise level 1.4 ± 0.1 dB over the entire frequency band).
(d) Tectronix TDS 420 digital storage oscilloscope connected by a general purpose interface bus to an IBM PC.

EMR is measured inside a thick-walled steel pressure vessel to render the artificial noise level negligible. For this purpose special radio-frequency filters are also used; power supply for the amplifier is independent of the industrial net, and special double-screen cables (Alpha wire corporation Ltd) are used to connect the antenna via the amplifier to the storage oscilloscope. The entire antenna–amplifier–storage oscilloscope system is completely adjusted to an input–output impedance of 50 Ω. The antenna is placed 2 cm from the centre of the loaded samples with its normal perpendicular to the cylinder axis that was parallel to the maximal loading direction (direction of crack propagation).

The loop antenna has no resonant frequency in the frequency range we measure. In this range it is characterized by a linear response of the form

$$E = k\frac{A_0}{h}, \qquad h = \frac{NS\omega}{c}, \tag{5}$$

where E is the field intensity, A_0 is the measured pulse maximum amplitude, the number of turns $N = 1$, $S = \pi D^2/4$ is the loop area ($D = 3$ cm), and c is the EMR propagation velocity; k is a geometrical factor which includes the solid angle of the antenna at the crack, the attenuation of the radiation in the material, etc.

The experiments were carried out on glass ceramics [18] and chalk samples taken from Horsha Foundation in the Beer Sheva syncline (south Israel) [19].

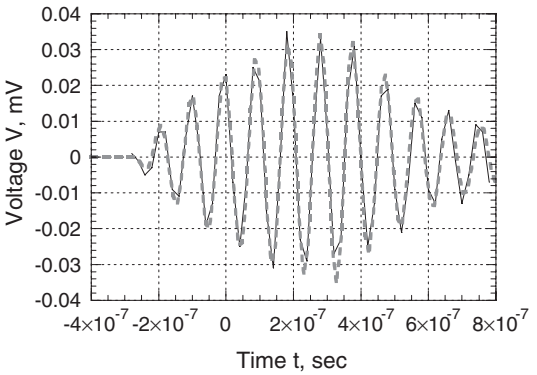

Figure 1. Experimental EMR pulse emitted from chalk with the following fitted parameters: $A_0 = 0.041 \pm 0.002$ mV, $\tau = 3 \times 10^{-7} \pm 0.27 \times 10^{-8}$ s, $t_0 = -2.683 \times 10^{-7} \pm 9 \times 10^{-10}$ s, $T = 3.4 \times 10^{-7} \pm 2 \times 10^{-8}$ s, $\omega = 6.59 \times 10^7 \pm 1 \times 10^5$ s^{-1}.

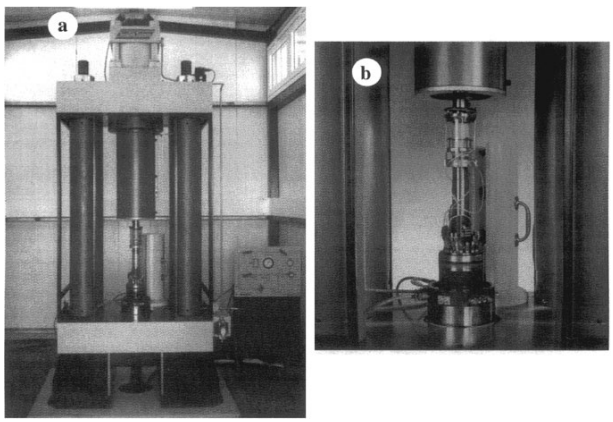

Figure 2. Compression press: (a) the triaxial load frame, (b) the sample stack.

3. Theoretical

Complicated EMR pulse shapes were analysed under the assumption that each pulse is a sum of two (or more) pulses. For example, in such an analysis a double signal consisting of two single pulses is characterized by ten parameters: two maximum amplitudes A_{01} and A_{02}, two rise and fall times τ_1 and τ_2, two frequencies ω_1 and ω_2, two pulse onset times t_{01} and t_{02} and two times of maximum amplitude T_1 and T_2. These are evaluated by the least-square method, although actually we can estimate most of the above parameters quite accurately before we begin the fitting procedure.

The first step is a Fourier transform (see figure 3) from which the two frequencies are estimated. These frequencies actually remain almost unchanged during the fitting process. The pulse onset times (t_{01} and t_{02}) are obtained from the graph of the signal versus time (e.g. figure 4): t_{01} is the x coordinate of the point where the oscillations begin, and t_{02} is the point where a deviation from a simple single pulse form is observed. These parameters also experience only minor changes during the fitting process.

The times to reach the envelope maxima are also estimated from the same graph as the x coordinates of the points where the pulse reaches its maxima: at least one of them is estimated quite accurately. Maximum amplitudes assume a plus or minus sign,

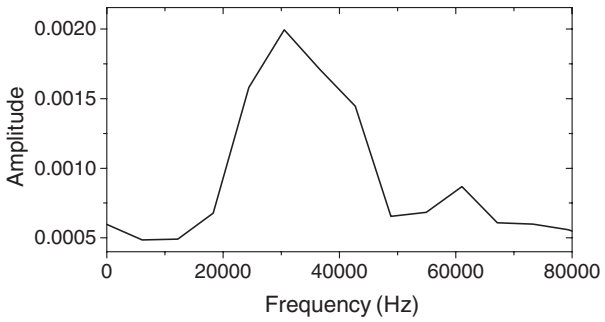

Figure 3. An example of frequency spectrum of a double pulse.

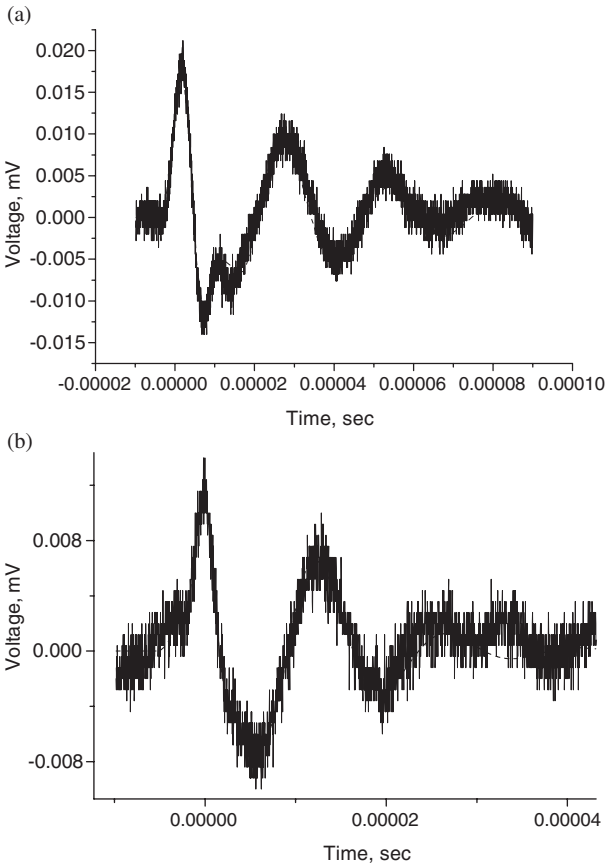

Figure 4. Examples of actual double pulses in chalk: (a) sequence of type (1), (b) sequence of type (2).

if the relevant oscillation starts in the upward or downward direction. Their values are estimated as maximum heights. Generally, the fitted values turn out to be somewhat greater than this initial estimation. The (equal) rise and fall times τ_1 and τ_2 for the two pulses are estimated from the graph as the times required for a pulse amplitude to decay by a factor e. They can be estimated from the graph (figure 4), especially the second one. Therefore, only two to four parameters, i.e. T_2, τ_1 and, possibly, A_{01} and A_{02} are estimated somewhat less accurately and need a more accurate least-square fitting. This fact actually limits the possibility of being 'trapped' at a local minimum in the least-square search.

Two types of double signal were observed:

(1) The first pulse begins at t_{01} and reaches its maximum at T_1; after the first pulse has passed its maximum, the second pulse begins at t_{02} and reaches its maximum at T_2, i.e. the second crack starts after the first one halts.

(2) The first pulse begins at t_{01}; then, before it reaches its maximum, the second pulse begins at t_{02} and reaches its maximum at T_2; only after that does the maximum of the first pulse T_1 occur. Thus, the implication is that the second crack both starts and stops during the evolution of the first one.

Let us consider, for example, a double pulse corresponding to case (1). The equation describing this signal has the following form:

$$A(t) = \begin{cases} A_{01}\sin\omega_1(t-t_{01}) \\ \quad \times\left[1-\exp\left(-\dfrac{t-t_{01}}{\tau_1}\right)\right], & t_{01} < t < T_1 \\ A_{01}\sin\omega_1(t-t_{01}) \\ \quad \times\left[1-\exp\left(-\dfrac{T_1-t_{01}}{\tau_1}\right)\right] \\ \quad \times\exp\left(-\dfrac{t-T_1}{\tau_1}\right), & T_1 < t < t_{02} \\ A_{01}\sin\omega_1(t-t_{01}) \\ \quad \times\left[1-\exp\left(-\dfrac{T_1-t_{01}}{\tau_1}\right)\right] \\ \quad \times\exp\left(-\dfrac{t-T_1}{\tau_1}\right) \\ \quad + A_{02}\sin\omega_2(t-t_{02}) \\ \quad \times\left[1-\exp\left(-\dfrac{t-t_{02}}{\tau_2}\right)\right], & t_{02} < t < T_2 \\ A_{01}\sin\omega_1(t-t_{01}) \\ \quad \times\left[1-\exp\left(-\dfrac{T_1-t_{01}}{\tau_1}\right)\right] \\ \quad \times\exp\left(-\dfrac{t-T_1}{\tau_1}\right) \\ \quad + A_{02}\sin\omega_2(t-t_{02}) \\ \quad \times\left[1-\exp\left(-\dfrac{T_2-t_{02}}{\tau_2}\right)\right] \\ \quad \times\exp\left(-\dfrac{t-T_2}{\tau_2}\right), & t > T_2. \end{cases} \tag{6}$$

The appearance of a double pulse may indicate a fracture process where either two cracks propagate sequentially or crack development differs from a uniform propagation of a rectangular crack, such as crack broadening. More complicated signals, e.g. triple ones consisting of three single pulses, can be similarly described.

4. Results and discussion

Two EMR pulses emitted by cracks in glass ceramics are analysed. The first pulse is a triple one. This triple EMR signal consists of a main, relatively long and strong pulse of low frequency, onto which two small pulses of higher frequencies are superimposed (figure 5), implying that during

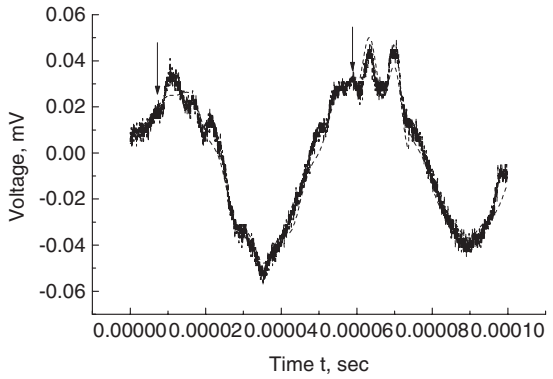

Figure 5. Experimental triple pulse emitted by a crack in glass ceramics (solid curve) with the fitting curve (dashed curve). Fitting parameters are: $T_1' = 96\ \mu$s, $\omega_1 = 1.15 \times 10^5\ \text{s}^{-1}$ (corresponding to the main crack); $T_2' = 20.4\ \mu$s, $\omega_2 = 8.125 \times 10^5\ \text{s}^{-1}$, $T_3' = 15.3\ \mu$s, $\omega_3 = 9.42 \times 10^5\ \text{s}^{-1}$ (these two correspond to smaller cracks). The origins of the secondary pulses are shown by arrows.

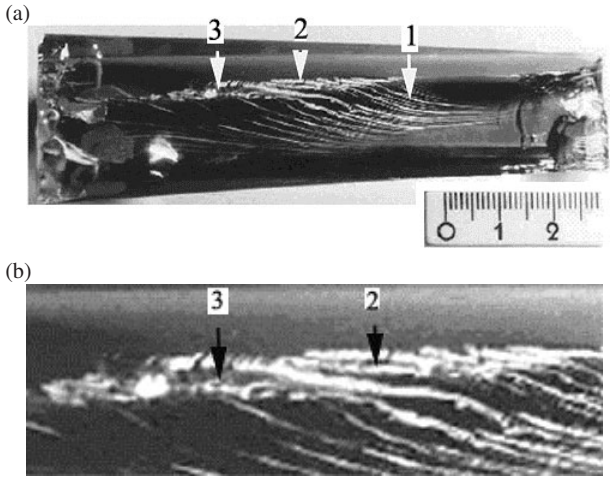

Figure 6. (a) Photograph of the crack in glass ceramics which emitted the triple pulse shown in figure 5. Initial striae on the main crack are marked by 1 and the striae continuations by 2 and 3. (b) Enlarged view of the two striae continuations. The striae continuations are misaligned with respect to the initial striae, and therefore the distinction of 2 and 3 is not very clear.

the propagation of the main crack two smaller cracks were initiated and halted one after another. The transparency of glass ceramics makes it possible to check this suggestion fractographically. A photograph of the main crack which is marked extensively by striae (numbered 1) is shown in figure 6(a) revealing, indeed, the presence of two striae extensions (numbered 2 and 3) besides those on the main crack (figure 6(b)). To calculate the crack dimensions from EMR signals, equations (2) and (3) of [18] were used. Those describe the relations between T' and L and between ω and b for glass ceramics: $T' = 8.15 \times 10^{-7} L$; $\omega = 2593\,700/b$. The directly measured dimensions of the main crack (no 1 in table 1) are 93 mm × 18 mm, while the values calculated by EMR signals are $L_1 = 118$ mm and $b_1 = 22.5$ mm respectively. The measured dimensions of the smaller cracks (nos 2 and 3 in table 1) are 20 mm × 2 mm and 24 mm × 1.5 mm, while the calculated values are $L_2 = 25$ mm, $b_2 = 3.2$ mm, $L_3 = 19$ mm and $b_3 = 2.8$ mm respectively.

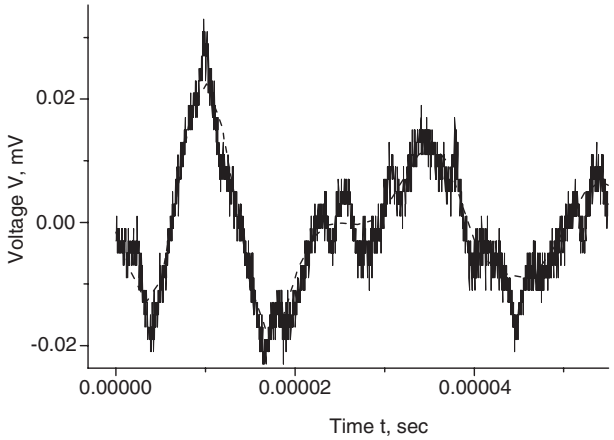

Figure 7. Double pulse emitted by a stress-relaxation crack in glass ceramics; its fitting parameters are: $T_1' = 84.6\ \mu$s, $\omega_1 = 4.22 \times 10^5\ \text{s}^{-1}$, corresponding to the earlier, smaller crack, and $T_2' = 20.4\ \mu$s, $\omega_2 = 3.39 \times 10^5\ \text{s}^{-1}$, which corresponds to the larger crack.

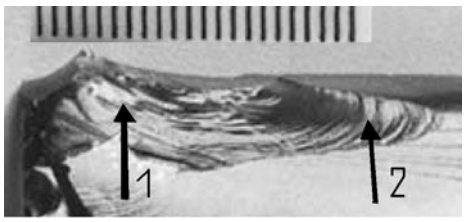

Figure 8. Photograph of the crack in glass ceramics which emitted the double pulse shown in figure 7.

The second double pulse analysed here (see figure 7) was emitted by the stress-relaxation crack of the same sample. This crack consists of two parts (figure 8); the smaller one (no 1 in table 1) appeared earlier (its measured dimensions were 7.5 mm × 3 mm), while the dimensions of the larger one (no 2 in table 1) were 15 mm × 4 mm. The dimensions obtained by a calculation from the EMR pulse are $L_1 = 10$ mm, $b_1 = 6$ mm for the first crack and $L_2 = 25$ mm and $b_2 = 8$ mm for the second. Note that by 'crack length' we imply the dimension in the crack propagation direction, while 'crack width' is the dimension normal to its propagation. Thus, the crack length is not always larger than the crack width.

For the above two signals, the correspondence for lengths is good, as well as for the widths of the first pulse. The measured and calculated values of the widths of some of the smaller cracks differ by a factor of 2. This difference may be due to the fact that here the cracks were open on one side (see equation (4)), and thus $b_1' = b_1/2 = 3$ mm and $b_2' = b_2/2 = 4$ mm respectively, which correspond exactly to the measured widths. Unfortunately, the question whether the crack is closed or open on one side cannot be solved by means of EMR alone; so an uncertainty of a factor of 2 in defining crack widths still remains. Thus, with the exception of the widths of smaller cracks, we can characterize quite well two types of crack superposition, triple and double pulses, where our calculations are verified by fractographic measurements.

While in glass ceramics the striae formed by mixed mode I and III loading [20] are sharp and continuous (figure 6(a)), in grainy materials (e.g. rocks, metals) these features are

Table 1. Complicated cracks in glass ceramics (shown in figures 3 and 5): dimensions measured and calculated from the fitted parameters of the triple EMR pulse shown in figure 2 and the double EMR pulse shown in figure 4. For the triple pulse, crack no 1 is the main crack, while cracks nos 2 and 3 are small side cracks. For the double pulse, the subcracks are numbered 1 and 2 in the order of their appearance.

	Crack no	Dimension	Measured (mm)	Calculated (mm)
Signal from figure 6	1	Length L_1	93	118
		Width b_1	18	22.5
	2	Length L_2	20	25
		Width b_2	2	3.2 ($b'_2 = 1.6$)
	3	Length L_3	24	20
		Width b_3	1.5	2.8 ($b'_3 = 1.4$)
Signal from figure 4	1	Length L_1	7.5	10
		Width b_1	3	6 ($b'_1 = 3$)
	2	Length L_2	15	25
		Width b_2	4	8 ($b'_2 = 4$)

Table 2. Selected EMR parameters of the double EMR pulses emitted during uniaxial compression failure of chalk and calculated areas of the emitting cracks. (Note that T' is related to crack length, while the pulse frequency is related to crack width.) The last column shows loading conditions: A, uniaxial ($\sigma_1 = 47.6$ MPa, $\sigma_3 = 0$); B, uniaxial ($\sigma_1 = 45.2$ MPa, $\sigma_3 = 0$); C, triaxial ($\sigma_1 = 47.6$ MPa, $\sigma_3 = 1$ MPa) [20].

Pulse no (single pulse no i)	Beginning t_{0i} (s)	End T_i (s)	T'_i (s)	Frequency ω_i (s^{-1})	Area (cm^2)	Pulse type	Loading condition
1(1)	0	7.82×10^{-6}	7.82×10^{-6}	432 750	1.8	(1)	A
1(2)	9.66×10^{-6}	1.026×10^{-5}	7.46×10^{-6}	236 950	3.15		
2(1)	0	8.52×10^{-6}	8.52×10^{-6}	406 800	2	(1)	A
2(2)	1.026×10^{-5}	2.296×10^{-5}	1.27×10^{-5}	233 750	5		
3(1)	0	4.07×10^{-6}	4.07×10^{-6}	309 250	1.3	(1)	A
3(2)	8.97×10^{-6}	4.536×10^{-5}	3.64×10^{-5}	184 200	19		
4(1)	0	3.35×10^{-5}	3.35×10^{-5}	232 050	14.5	(2)	A
4(2)	4.37×10^{-6}	1.331×10^{-5}	8.94×10^{-6}	463 750	1.9		
5(1)	0	7.2×10^{-6}	7.2×10^{-6}	389 750	1.85	(1)	A
5(2)	1.08×10^{-5}	1.976×10^{-5}	8.97×10^{-6}	241 800	3.7		
6(1)	0	1.564×10^{-5}	1.564×10^{-5}	435 100	3.6	(2)	B
6(2)	3.3×10^{-6}	6.51×10^{-6}	3.22×10^{-6}	904 700	0.36		
7(1)	0	1.446×10^{-5}	1.446×10^{-5}	463 350	3	(2)	B
7(2)	2.59×10^{-6}	6.99×10^{-6}	4.4×10^{-6}	936 000	0.5		
8(1)	0	4.93×10^{-6}	4.93×10^{-6}	730 300	0.67	(1)	B
8(2)	5.82×10^{-6}	9.62×10^{-6}	3.8×10^{-6}	504 350	0.75		
9(1)	0	1.38×10^{-6}	1.38×10^{-6}	2046 000	0.07	(1)	C
9(2)	2.1×10^{-6}	3.33×10^{-6}	1.23×10^{-6}	1170 000	0.1		
10(1)	0	1.55×10^{-6}	1.55×10^{-6}	2030 000	0.08	(1)	C
10(2)	2.18×10^{-6}	3.33×10^{-6}	1.15×10^{-6}	1210 900	0.1		
11(1)	0	1.29×10^{-6}	1.29×10^{-6}	2106 700	0.06	(1)	C
11(2)	2.04×10^{-6}	3.29×10^{-6}	1.25×10^{-6}	1191 400	0.1		

divided into many microcracks, sharpness is lost and replaced by a fussy morphology. Therefore, in such grainy materials the identification of specific cracks becomes difficult or impossible. Accordingly, in chalk samples no clear correlation between specific cracks and EMR pulses was possible, and resort to the correlation obtained for glass ceramics (figures 5–8) was made as a method to interpret the EMR results there.

In the compression experiments on chalk, double pulses frequently emanated near the peak of the stress–strain curve. The same analytical method as presented above was applied to 11 double pulses obtained from deformed chalk samples (figures 9(A)–(C)). Each pulse is depicted by two black arrows, their beginnings and ends corresponding to the times of the initiation and termination of the cracks respectively. Thus, the length of each arrow gives the time duration of the corresponding crack propagation and is, therefore, proportional to its length. The width of each arrow is inversely proportional to the frequency and is, therefore, proportional to the corresponding (EMR calculated) crack width. Note that for eight pulses the second part begins after the first one ends, which corresponds to case (1) (see also table 2); an example of this sequence is shown in figure 4(a). In the remaining three pulses (4, 6, 7 in table 2) the second part starts and terminates before the first is over, which corresponds to case (2); an example of this sequence is shown in figure 4(b). The parameters of the pulse shown in figure 4(b) are: $A_{01} = 0.01$ mV, $A_{02} = 0.009$ mV, $\tau_1 = 8.77$ μs, $\tau_2 = 1.17$ μs, $\omega_1 = 4.35 \times 10^5$ s^{-1}, $\omega_2 = 9.05 \times 10^5$ s^{-1}, $t_{01} = -5.31$ μs,

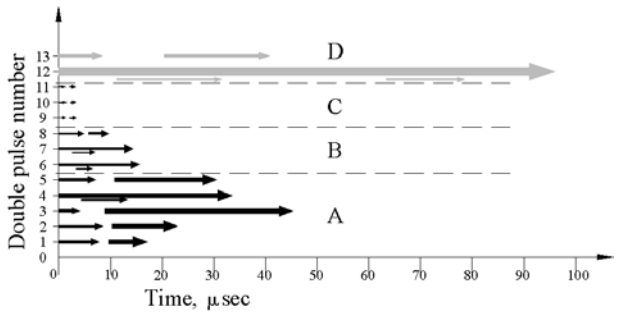

Figure 9. Description of all double pulses observed in chalk: each double pulse is shown by two black arrows corresponding to the single pulses constituting the double pulse; dashed horizontal lines separate the pulses emitted by different chalk samples denoted by (A)–(C). Triple and double pulses emitted by glass ceramics (see also figures 5 and 7) are also shown for comparison by grey arrows (D).

$t_{02} = -2.02\,\mu$s, $T_1 = 10.32\,\mu$s, $T_2 = 1.2\,\mu$s. It also turned out that the three shorter signals (nos 9–11 in figure 9) were emitted by the sample under triaxial compressional loading, namely a confining radial stress acting normal to the axial stress, while in two other samples the loading was uniaxial. For the sake of comparison, figure 9 also shows the signals emanating from glass ceramics (by grey arrows).

All double pulses in chalk correspond to cracks with calculated areas ranging from 20 mm^2 to 20 cm^2. That is, they are emitted by 'large' cracks ('small' cracks are those with areas below 1 mm^2). Moreover, they occur at late stages of the sample loading. Reciprocally, none of the pulses from large cracks is single, leading to the conclusion that all large cracks in chalk are, in fact, double. This result, as well as the order and exact timing of the pairs of cracks can only be gleaned by EMR.

5. Conclusions

Extension of the model of EMR to complex cases has been presented. It is shown that complex EMR pulses carry information about crack propagation details, such as the time sequence, in addition to crack dimensions. The EMR analysis is therefore a useful tool for understanding complex fracture processes, which can shed light on multiple fracturing, as well as on narrowing or broadening of propagating single fractures.

Acknowledgments

This research no 93/02-1 was supported by the Israel Science Foundation.

The authors are grateful to B Goldbaum for useful discussions and to L Baluashvili for technical help. Thanks are due to George Beall for supplying the glass ceramic sample.

References

[1] Urusovskaja A A 1969 Electric effects associated with plastic deformation of ionic crystals *Sov. Phys.—Usp.* **11** 631–43

[2] Misra A 1975 Electromagnetic effects at metallic fracture *Nature* **254** 133–4

[3] Nitsan U 1977 Electromagnetic emission accompanying fracture of quartz-bearing rocks *Geophys. Res. Lett.* **4** 333

[4] Khatiashvili N G and Perel'man M E 1989 On the mechanism of seismo-electromagnetic phenomena and their possible role in the electromagnetic radiation during periods of earthquakes, foreshocks and aftershocks *Phys. Earth Planet. Inter.* **57** 169–77

[5] Fifolt D A, Petrenko V F and Schulson E M 1993 Preliminary study of electromagnetic emissions from cracks in ice *Phil. Mag.* B **67** 289–99

[6] Miroshnichenko M and Kuksenko V 1980 Emission of electromagnetic pulses during nucleation of cracks in solid insulators *Sov. Phys.—Solid State* **22** 895–6

[7] Warwick J W, Stoker C and Meyer T R 1982 Radio emission associated with rock fracture: possible application to the Great Chilean earthquake of May 22, 1960 *J. Geophys. Res.* **87** 2851–9

[8] Rabinovitch A, Frid V, Bahat D and Goldbaum J 2000 Fracture area calculation from electromagnetic radiation and its use in chalk failure analysis *J. Rock Mech. Mining Sci.* **37** 1149–54

[9] Rabinovitch A, Bahat D and Frid V 1995 Comparison of electromagnetic radiation and acoustic emission in granite fracturing *Int. J. Fract.* **71** R33–41

[10] Rabinovitch A, Frid V and Bahat D 1998 Parametrization of electromagnetic radiation pulses obtained by triaxial fracture of granite sample *Phil. Mag. Lett.* **77** 289–93

[11] Rabinovitch A, Frid V and Bahat D 1999 A note on the amplitude–frequency relation of electromagnetic radiation pulses induced by material fracture *Phil. Mag. Lett.* **79** 195–200

[12] Rabinovitch A, Frid V and Bahat D 1996 Emission of electromagnetic radiation by rock fracturing *Z. Geol. Wiss.* **24** 361–8

[13] Frid V, Bahat D, Goldbaum J and Rabinovitch A 2000 Experimental and theoretical investigations of electromagnetic radiation induced by rock fracture *Isr. J. Earth-Sci.* **49** 9–19

[14] Goldbaum J, Frid V, Rabinovitch A and Bahat D 2001 Electromagnetic radiation induced by percussion drilling *Int. J. Fract.* **111** L15–20

[15] Frid V, Rabinovitch A and Bahat D 1999 Electromagnetic radiation associated with induced triaxial fracture in granite *Phil. Mag. Lett.* **79** 79–86

[16] Rabinovitch A, Frid V, Bahat D and Goldbaum J 2003 Decay mechanism of the fracture induced electromagnetic pulses *J. Appl. Phys.* **90** 5085–90

[17] Rabinovitch A, Frid V, Bahat D and Goldbaum J 2002 *IUTAM Symp. on Analytical and Computational Fracture Mechanics of Non-Homogeneous Materials* ed B L Karihaloo (London: Kluwer Academic) pp 343–8

[18] Bahat D, Frid V, Rabinovitch A and Palchik V 2002 Exploration via electromagnetic radiation and fractographic methods of fracture properties induced by compression in glass ceramics *Int. J. Fract.* **116** 179–94

[19] Bahat D 1991 *Tectonofractography* (Heidelberg: Springer)

[20] Lawn B 1993 *Fracture of Brittle Solids* (Cambridge: Cambridge University Press)

[21] Bahat D, Rabinovitch A and Frid V 2001 Fracture characterization of chalk in uniaxial and triaxial tests by rock mechanics, fractographic and electromagnetic radiation methods *J. Struct. Geol.* **23** 1531–47